Korea-Australia Rheology Journal
Vol. 16, No. 4, December 2004 pp. 201-212

Modeling of rheological behavior of nanocomposites by Brownian dynamics simulation

Young Seok Song and Jae Ryoun Youn*
School of Materials Science and Engineering, Seoul National University, 56-1, Shinlim-Dong, Gwanak-Gu, Seoul 151-744, Korea
(Received December 1, 2004)

Abstract

Properties of polymer based nanocomposites depend on dispersion state of embedded fillers. In order to examine the effect of dispersion state on rheological properties, a new bi-mode FENE dumbbell model was proposed. The FENE dumbbell model includes two separate ensemble sets of dumbbells with different friction coefficients, which simulate behavior of well dispersed and aggregated carbon nanotubes (CNTs). A new parameter indicating dispersion state of the CNT was proposed to account for degree of dispersion quantitatively as well as qualitatively. Rheological material functions in elongational, steady shear, and oscillatory shear flows were obtained numerically. The CNT/epoxy nanocomposites with different dispersion state were prepared depending on whether a solvent is used for the dispersion of CNTs or not. Dispersion state of the CNT in the epoxy nanocomposites was morphologically characterized by the field emission scanning electronic microscope and the transmission electron microscope images. It was found that the numerical prediction was in a good agreement with experimental results especially for steady state shear flow.

Keywords : nanocomposites, FENE dumbbell, carbon nanotubes, rheology

1. Introduction

Polymer based nanocomposites filled with carbon nanotubes (CNTs) have been studied to achieve superior electrical, thermal, and mechanical properties compared with composites filled with other carbon nanomaterials (CNMs) like carbon blacks (CBs) (Allaoui *et al.*, 1993). The outstanding properties are attributed to the high aspect ratio which is generally higher than 1000. In order to achieve optimal enhancement in the property of the CNT/polymer composites, there are several key issues to be resolved, i.e., improved dispersion of CNTs, alignment of CNTs in the polymer resin, and functionalization of the CNT surface for good adhesion. In order to disperse CNTs in the polymer homogeneously, modification of pristine CNT surface such as chemical or plasma treatments has been carried out (Shaffer *et al.*, 1998).

It is necessary to understand rheological behavior of the CNT/polymer mixture so as to improve manufacturing procedure of the nanocomposites. There are a few reports on rheological behavior of CNT/polymer composites. Pötschke *et al.* (2002) investigated rheological properties of the CNT/polycarbonate (PC) composites. It was found that increase in the viscosity of the nanocomposites filled with CNTs was much higher than increase in the viscosity of polymer composites filled with carbon fibers or CBs. The rheological behavior of aqueously dispersed CNTs was studied by Kinloch *et al.* (2002) under consideration of the interaction between the nanotubes. They reported that dispersion state of the CNT was highly sensitive to the strain applied in the linear viscoelastic region and the storage and loss moduli were independent of frequency. It was shown that viscosity increased to the highest point when fibrous fillers such as carbon fibers were added and to the lowest point when spherical fillers were added. Agglomerates of the fillers caused higher viscosity (Shenoy, 1999) since the presence of agglomerates leads to apparent higher filler loading. It was found that the nanocomposites filled with functionalized CNTs had better dispersion of the CNT and showed higher storage modulus and complex viscosity at low frequency. On the other hand, it hasn't been numerically investigated how the dispersion state of the CNT affects various properties of the nanocomposites. In this study, the effect of the CNT dispersion on rheological behavior was examined based on a proposed bi-mode FENE (finitely extensible nonlinear elastic) dumbbell model.

Dynamic behavior of polymeric solutions is an area of great interest in the field of polymer science (Larson, 1988). However, the size and complexity of polymer mol-

*Corresponding author: jaeryoun@snu.ac.kr

ecules prohibit use of realistic polymer models. Therefore, molecular theories of polymers have concentrated on the simple models that include only the most basic characteristics of polymer molecules. The model used frequently is a dumbbell model which consists of beads and springs. This study also adopted the dumbbell model to describe rheological behavior of the CNT/polymer composites quantitatively as well as qualitatively. Microstructural modeling of the nanocomposites was conducted using Brownian dynamics simulation which is a very powerful tool for understanding the dynamics of polymers both at equilibrium and during undergoing flow. Originally, the simulation is based on numerical integration of the equations of motion for the beads of a single chain molecule, where presence of Brownian or random forces implies that the equations of motion become stochastic differential equations. The diffusion equations for suitable configurational distribution of the dumbbells, which are often referred to as Fokker-Planck equations, are equivalent to stochastic differential equations. Numerical integration of the stochastic differential equations leads to stochastic simulation, which is known to be so simple that even complicated problems can be treated without much efforts.

Warner (1972) proposed a FENE dumbbell model and calculated steady shear flow and small amplitude oscillatory flow by using the model. He found that various material functions varied between Hookean spring and rigid dumbbell. Christiansen and Bird (1977; 1978) compared experimental results for intrinsic viscosity and intrinsic complex viscosity with values predicted by the FENE dumbbell and showed that the FENE dumbbell adequately predicted the intrinsic viscosity, but less successfully portrayed the behavior in small amplitude oscillatory motion. Armstrong and Ishikawa (1980) adopted nearly-Hookean dumbbells and showed substantial improvements over Hookean dumbbell predictions. They used perturbation scheme to obtain an expression for the stress tensor. Bird and Deaguiar (1983) employed an encapsulated FENE dumbbell model for concentrated solutions and melts in the case where the Brownian motion and hydrodynamic forces acting on the beads were made anisotropic. Bird and Wiest (1985) modified kinetic theory for suspensions of elastic dumbbells by introducing anisotropic hydrodynamic drag and anisotropic Brownian motion. Fan (1985) improved rheological features of FENE dumbbells in dilute suspension undergoing steady-state shear flow by assuming a distribution function to remove the singularity and improve behavior of the weight function in the Galerkin expression. Schieber (1993) proposed a noninertial Hookean dumbbell with internal viscosity in transient and steady shear flows by using Gaussian closure on the second moment equation of the dumbbell configuration, which greatly overestimated the relative stretching of the polymer coil. Herrchen and Öttinger (1997) compared three dumbbell models, i.e., original FENE model with the Warner spring force, FENE-P model based on the Peterlin approximation, and FENE-CR model as suggested by Chilcott and Rallison. Vaccaro and Marrucci (2000) developed a model for the impermanent network of associating telechelic chain which incorporated the basic molecular mechanisms and obtained an analytical expression for the viscosity at low shear rates. Hernández Cifre *et al.* (2003) employed two kinds of ensembles of dumbbells which consist of active and dangling chains, to model reversible network of associative chains.

As mentioned above, there have been many studies on modeling rheological properties and outstanding results using Brownian dynamic simulations for pure polymer solutions or melts. However, few studies on theoretical modeling of rheological properties of nanocomposites have been reported. In this study, rheological properties of CNT/epoxy composites were characterized by experimental measurements and a new bi-mode FENE dumbbell model was proposed to predict rheological behavior of the nanocomposites.

2. Experimental

2.1. Materials and preparation of CNTs/epoxy composites

Multiwalled carbon nanotubes (MWNTs) used in this study were supplied by Iljin Nanotech Co. The CNTs synthesized by the chemical vapor deposition (CVD) process have the average diameter of 13 nm and the length of 10 μm. Epoxy resin was selected as the polymer matrix because it is known that the CNTs are dispersed well in the epoxy resin compared with other polymer resins. Epoxy resin (YD 128) and hardener (TH 432) were obtained from the Kukdo Chemical, based on diglycidyl ether of bisphenol-A and modified aromatic amine, respectively. The CNTs prepared were composed of many aggregates of different sizes. The aggregates would be obstacles to uniform dispersion of the MWNTs and were hardly broken into individual tubes in the epoxy resin. The epoxy composites containing well dispersed CNTs were prepared by the following procedures. The CNTs of 0.5, 1.0 and 1.5 wt% were first dispersed in ethanol, under sonication for 2 hours. The CNT/ethanol solutions with different CNT weight fractions were then mixed with the epoxy resin. The mixture was also sonicated for 1 hour at 80°C and kept in a vacuum oven for 5 days to remove air bubbles and the ethanol. After adding the hardener, the mixture was stirred by using a magnetic bar for 15 minutes under sonication. On the other hand, the poorly dispersed CNT/epoxy composites were prepared under sonication for 3 hours without using the solvent. It was expected that relatively well dispersed CNT nanocomposites could be obtained when the solvent was employed in the CNT dispersion process.

However, without using the solvent, the aggregates of pristine CNTs could remain in the polymer matrix. The quality of dispersion was verified by FESEM and TEM observations.

2.2. Rheological measurements

Dynamic rheological measurement was carried out by using a stress controlled rotational rheometer (C-VOR from Bohlin instrument Ltd). The measurement was conducted in an oscillatory shear mode using a parallel plate geometry at 25°C. Stress sweep tests were performed to identify linear viscoelastic regime. Shear stress was fixed at 1 Pa during all frequency sweep tests and sample thickness was set to be 1 mm. Steady shear test was also performed with another stress controlled rotational rheometer (AR2000). Cone and plate geometry was employed to obtain steady-state shear viscosity and first normal stress coefficient.

2.3. Morphological characterization

FESEM images were obtained with JEOL JSM-6330F operating at 5 kV to examine surfaces of the specimens fractured during tensile test. They were coated with Pt for 5 minutes prior to the observation. In addition to FESEM, TEM observation was carried out with JEOL JEM-2000EXII at 100 kV for more exact characterization of the morphology. The TEM specimens were microtomed to an ultra thin section with the thickness of about 80 nm and coated with carbon for 7 minutes to prevent the specimens from the degradation caused by the irradiation of electrons.

3. Microstructural modeling of nanocomposites

3.1. FENE dumbbells

FENE dumbbell model is appropriate for modeling dilute polymer solutions. It was assumed that the CNT/epoxy nanocomposites prepared in this study included CNTs of so low weight fraction that they could be thought as a dilute suspension of the CNTs in the epoxy matrix. In the bi-mode FENE dumbbell model, the FENE dumbbells are regarded as the CNTs instead of polymer chains. The main simplification of the bi-mode FENE dumbbell model is that aggregated and free FENE dumbbells can simulate rheological behavior for the CNT/epoxy composites that consists of the mixture of aggregated and well dispersed CNTs. It is proposed that the aggregated and free FENE dumbbells imitate the aggregated CNTs and well dispersed CNTs, respectively. The aggregated CNTs within polymer matrix have lower mobility than well dispersed CNTs which are also called free CNTs. The aggregated and free CNTs are modeled by two separate ensemble sets of FENE dumbbells as shown in Fig. 1. It is assumed that the aggregated and free FENE dumbbells do not interact each other and the total number of aggregated and free dumbbells is constant.

3.2. Bi-mode FENE dumbbell

The simplest method to simulate the polymer chain is to employ Hookean elastic dumbbell. Because the dumbbell model can be solved analytically, it has been used to develop constitutive equations. However, there are many limitations to the dumbbell model such as infinite elongational viscosity under a finite elongational rate. A solution to overcome these problems is to replace the Hookean spring by a non-linear elastic spring to limit the dumbbell extension to a maximum value, i.e., FENE spring introduced by Warner. In the FENE dumbbell model, connector force is written as below.

$$\boldsymbol{F}^c = \frac{H\boldsymbol{Q}}{1-(Q^2/Q_0^2)} \tag{1}$$

where Q_0 denotes the maximum possible spring extension. It is known that the model can describe the shear rate dependence of the shear viscosity well but not the complex viscosity quantitatively since it does not include sufficient internal motions of the macromolecules. A major drawback of the FENE model is that it does not yield a closed form constitutive equation for the polymer stress. The FENE kinetic theory involves a relaxation time $\lambda_H = \zeta/4H$ and a dimensionless finite extensibility parameter $b = HQ_0^2/kT$. In this study, b is fixed as 50, which is within the range of values that are consistent with the underlying kinetic framework. In order to simplify numerical calculations the following dimensionless quantities are employed.

$$\hat{\boldsymbol{Q}} = \boldsymbol{Q}/(k_BT/H)^{1/2}, \quad \hat{t} = t/\lambda_H, \quad \hat{\boldsymbol{\kappa}} = \boldsymbol{\kappa}\lambda_H, \quad \hat{\psi} = \psi((k_BT)/H)^{3/2} \tag{2}$$

By setting n_a as the number of aggregated dumbbells per unit volume and n_f as the number of free dumbbells per unit volume, total number density n is given as below.

$$n = n_a + n_f \tag{3}$$

A new parameter, c, is defined such that it represents degree of dispersion state of CNTs as follows.

$$\frac{n_a}{n} = c, \quad \frac{n_f}{n} = 1-c \tag{4}$$

The model built under the above assumptions is governed by a set of two Fokker-Planck equations. Let $\psi_a(\boldsymbol{Q}_a, t)$ and $\psi_f(\boldsymbol{Q}_f, t)$ be distribution functions describing the probability of finding aggregated and free dumbbells. Relations between these distribution functions and c are found to be

$$c = \int \psi_a dV, \quad 1-c = \int \psi_f dV \tag{5}$$

where dV denotes the volume element in $\boldsymbol{Q}$ space. The diffusion equation for the distribution function of aggregated dumbbells is given as

$$\frac{\partial \psi_a}{\partial t} = -\frac{\partial}{\partial \boldsymbol{Q}_a}\cdot\left(\boldsymbol{\kappa}\cdot\boldsymbol{Q}_a\psi_a - \frac{2}{\zeta_a}\boldsymbol{F}_a^c\psi_a\right) + \frac{2k_BT}{\zeta_a}\frac{\partial}{\partial \boldsymbol{Q}_a}\cdot\frac{\partial}{\partial \boldsymbol{Q}_a}\psi_a \tag{6}$$

where ζ_a is the friction coefficient of aggregated dumbbells, k_B is the Boltzmann constant, and T is the temperature. Since homogeneous flows are considered, the velocity field can be written as $\boldsymbol{v} = \boldsymbol{\kappa} \cdot \boldsymbol{r}$ where $\boldsymbol{\kappa} = (\nabla \boldsymbol{v})^T$. The evolution equation for the distribution function of free dumbbell is written as

$$\frac{\partial \psi_f}{\partial t} = -\frac{\partial}{\partial \boldsymbol{Q}_f} \cdot \left(\boldsymbol{\kappa} \cdot \boldsymbol{Q}_f \psi_f - \frac{2}{\zeta_f} \boldsymbol{F}_f^c \psi_f \right) + \frac{2k_B T}{\zeta_f} \frac{\partial}{\partial \boldsymbol{Q}_f} \cdot \frac{\partial}{\partial \boldsymbol{Q}_f} \psi_f \tag{7}$$

where ζ_f is the friction coefficient of free dumbbells, which is lower than that of aggregated dumbbells. The Fokker-Planck equations are expressed in the following dimensionless forms based on the assumption that λ_H is equal to $\zeta_f/4H$.

$$\frac{\partial \hat{\psi}_a}{\partial \hat{t}} = -\frac{\partial}{\partial \hat{\boldsymbol{Q}}_a} \cdot \left(\hat{\kappa} \cdot \hat{\boldsymbol{Q}}_a \hat{\psi}_a - \frac{1}{2} \frac{\zeta_f}{\zeta_a} \hat{\boldsymbol{F}}_a^c \hat{\psi}_a \right) + \frac{1}{2} \frac{\zeta_f}{\zeta_a} \frac{\partial}{\partial \hat{\boldsymbol{Q}}_a} \cdot \frac{\partial}{\partial \hat{\boldsymbol{Q}}_a} \hat{\psi}_a \tag{8}$$

$$\frac{\partial \hat{\psi}_f}{\partial \hat{t}} = -\frac{\partial}{\partial \hat{\boldsymbol{Q}}_f} \cdot \left(\hat{\kappa} \cdot \hat{\boldsymbol{Q}}_f \hat{\psi}_f - \frac{1}{2} \hat{\boldsymbol{F}}_f^c \hat{\psi}_f \right) + \frac{1}{2} \frac{\partial}{\partial \hat{\boldsymbol{Q}}_f} \cdot \frac{\partial}{\partial \hat{\boldsymbol{Q}}_f} \hat{\psi}_f \tag{9}$$

It is found that Eq. (9) is equal to that of original FENE dumbbell model. When the Brownian motion is isotropic, the above pair of equations are equivalent to the Ito stochastic differential equations (SDE) for a three dimensional Markov process $\hat{\boldsymbol{Q}}$.

$$d\hat{\boldsymbol{Q}}_a = \left(\hat{\boldsymbol{\kappa}} \cdot \hat{\boldsymbol{Q}}_a - \frac{1}{2} \frac{\zeta_f}{\zeta_a} \frac{1}{1 - \hat{Q}_a^2/b} \hat{\boldsymbol{Q}}_a \right) d\hat{t} + \sqrt{\frac{\zeta_f}{\zeta_a}} d\boldsymbol{W}_a \tag{10}$$

$$d\hat{\boldsymbol{Q}}_f = \left(\hat{\boldsymbol{\kappa}} \cdot \hat{\boldsymbol{Q}}_f - \frac{1}{2} \frac{1}{1 - \hat{Q}_f^2/b} \hat{\boldsymbol{Q}}_f \right) d\hat{t} + d\boldsymbol{W}_f \tag{11}$$

where $\boldsymbol{W}$ is the three dimensional Wiener process. Since the non-linear SDEs cannot be solved analytically, numerical methods must be used to solve them. The second-order predictor-corrector algorithm suggested by Öttinger (1996) is adopted to calculate Eq. (10) and Eq. (11) as below.

$$\hat{\boldsymbol{Q}}'_{a,j+1} = \hat{\boldsymbol{Q}}_{a,j} + \left(\hat{\boldsymbol{\kappa}}_j \cdot \hat{\boldsymbol{Q}}_{a,j} - \frac{1}{2} \frac{\zeta_f}{\zeta_a} \frac{1}{1 - \hat{Q}_{a,j}^2/b} \hat{\boldsymbol{Q}}_{a,j} \right) \Delta\hat{t} + \sqrt{\frac{\zeta_f}{\zeta_a}} \Delta \boldsymbol{W}_j \tag{12}$$

$$\hat{\boldsymbol{Q}}_{a,j+1} = \hat{\boldsymbol{Q}}_{a,j} + \left(\begin{array}{l} \hat{\boldsymbol{\kappa}}_{j+1} \cdot \hat{\boldsymbol{Q}}_{a,j+1} - \dfrac{1}{2} \dfrac{\zeta_f}{\zeta_a} \dfrac{1}{1 - \hat{Q}_{a,j+1}^2/b} \hat{\boldsymbol{Q}}_{a,j+1} \\ + \hat{\boldsymbol{\kappa}}_j \cdot \hat{\boldsymbol{Q}}_{a,j} - \dfrac{1}{2} \dfrac{\zeta_f}{\zeta_a} \dfrac{1}{1 - \hat{Q}_{a,j+1}^2/b} \hat{\boldsymbol{Q}}_{a,j} \end{array} \right) \Delta\hat{t} + \sqrt{\frac{\zeta_f}{\zeta_a}} \Delta \boldsymbol{W}_j \tag{13}$$

$$\hat{\boldsymbol{Q}}'_{f,j+1} = \hat{\boldsymbol{Q}}_{f,j} + \left(\hat{\boldsymbol{\kappa}}_j \cdot \hat{\boldsymbol{Q}}_{f,j} - \frac{1}{2} \frac{1}{1 - \hat{Q}_{f,j}^2/b} \hat{\boldsymbol{Q}}_{f,j} \right) \Delta\hat{t} + \Delta \boldsymbol{W}_j \tag{14}$$

$$\hat{\boldsymbol{Q}}_{f,j+1} = \hat{\boldsymbol{Q}}_{f,j} + \left(\begin{array}{l} \hat{\boldsymbol{\kappa}}_{j+1} \cdot \hat{\boldsymbol{Q}}_{f,j+1} - \dfrac{1}{2} \dfrac{1}{1 - \hat{Q}_{f,j+1}^2/b} \hat{\boldsymbol{Q}}_{f,j+1} \\ + \hat{\boldsymbol{\kappa}}_j \cdot \hat{\boldsymbol{Q}}_{f,j} - \dfrac{1}{2} \dfrac{1}{1 - \hat{Q}_{f,j+1}^2/b} \hat{\boldsymbol{Q}}_{f,j} \end{array} \right) \Delta\hat{t} + \Delta \boldsymbol{W}_j \tag{15}$$

where $\Delta \boldsymbol{W}_j = \boldsymbol{W}_{j+1} - \boldsymbol{W}_j$. The magnitude of connect vectors determined by Eq. (12) to (15) is between 0 and $b^{1/2}$. For any given velocity gradient $\boldsymbol{\kappa}$, contribution of the dumbbells to the instantaneous stress tensor is calculated by means of weighted average over both the aggregated and free dumbbells based on the Kramers form expression.

$$\boldsymbol{\tau}_p = n_a \langle \boldsymbol{Q}_a \boldsymbol{F}_a^c \rangle + n_f \langle \boldsymbol{Q}_f \boldsymbol{F}_f^c \rangle_f - n k_B T \boldsymbol{\delta} \tag{16}$$

Total stress tensor is given by the following equation.

$$\boldsymbol{\tau} = \boldsymbol{\tau}_s + \boldsymbol{\tau}_p = \eta_s \dot{\boldsymbol{\gamma}} + \boldsymbol{\tau}_p \tag{17}$$

here $\boldsymbol{\tau}_s$ is the contribution by the solvent of the viscosity η_s.

In order to obtain more precise solutions in the stochastic simulations, it is necessary to implement variance reduction techniques. Recently, it has been reported that variance reduction techniques are applied to simulations of polymer dynamics (Öttinger, 1994). Fluctuation of the averaged stress tensor may occur at low flow rate. Parallel equilibrium simulation employing the same initial configurations and the same stochastic displacements is carried out. In order to solve the ζ_f/ζ_a Eq. (12) to (15), a ratio of friction coefficient, must be determined. The translational diffusivity D_{tr} defined by the Nernst-Einstein equation is related to the friction coefficient Z for the entire molecule as follows.

$$D_{tr} = \frac{k_B T}{Z} \tag{18}$$

According to phase-space theory (Bird *et al.*, 1987), when hydrodynamic interaction is neglected for the dilute solution, the translational diffusivity is also written as below.

$$D_{tr} = \frac{k_B T}{N\zeta} \tag{19}$$

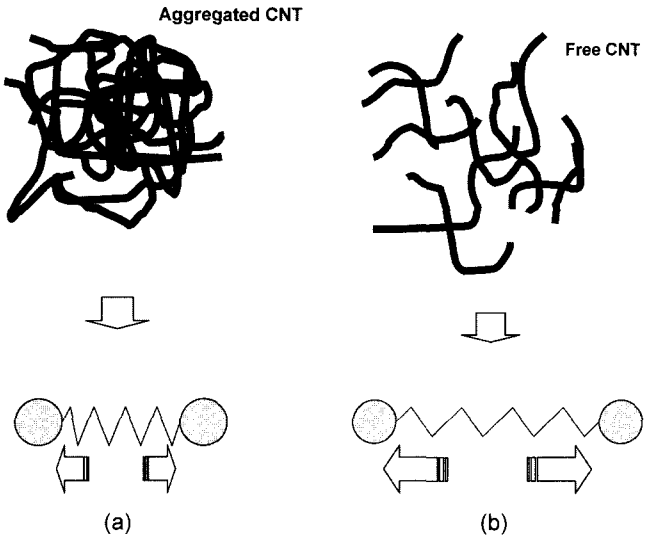

Fig. 1. Modeling of two kinds of dumbbell sets, (a) aggregated FENE dumbbell which has lower mobility and (b) free FENE dumbbell which has higher mobility.

For polymer melts or concentrated polymer solutions, the translational diffusivity is expressed as

$$D_{tr} = \frac{k_B T}{N^2 \zeta} \tag{20}$$

where N is 2 in the case of elastic dumbbell. Eq. (20) means that concentrated polymer solutions have lower diffusion, i.e., lower mobility than dilute solutions. Because the aggregated and free dumbbells copy the concentrated and dilute polymer solutions, it is assumed that ζ_f/ζ_a is equal to 0.5.

5. Results and discussion

5.1. Experimental results

5.1.1. Rheological properties

Fig. 2(a) and (b) show the storage modulus, G', for the epoxy composites filled with well dispersed CNTs and poorly dispersed CNTs. It is found that the storage modulus of the nanocomposite dramatically increases with

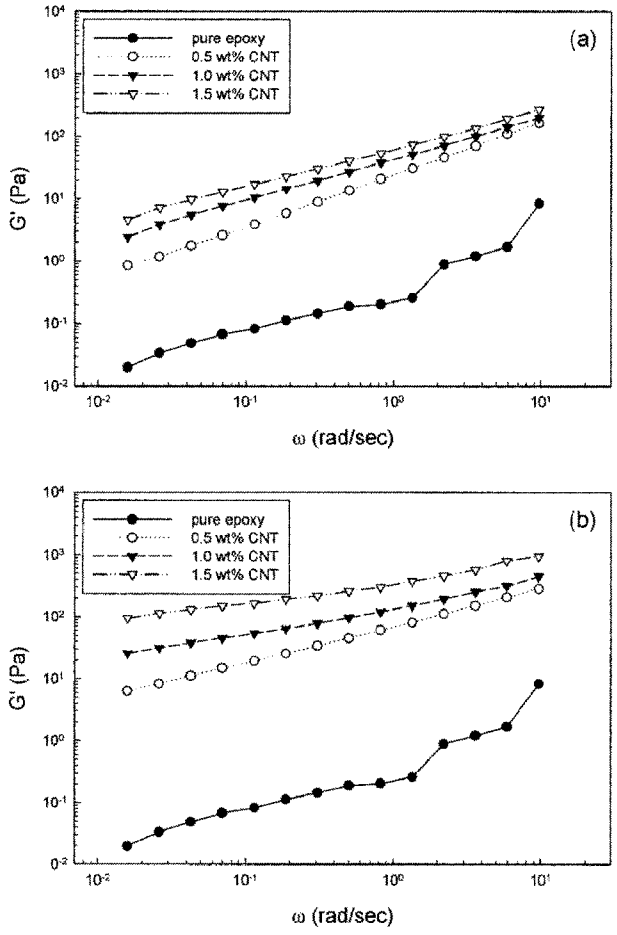

orage moduli of epoxy nanocomposites embedded with well dispersed CNTs and (b) poorly dispersed CNTs as nction of angular frequency.

Table 1. Terminal slopes of G' and G" for CNTs/epoxy composites prepared (a) with the solvent and (b) w. the solvent

(a)

Samples	Slope of G'	Slope of G"
0.5 wt% CNT	0.83	0.88
1.0 wt% CNT	0.67	0.80
1.5 wt% CNT	0.61	0.76

(b)

Samples	Slope of G'	Slope of G"
0.5 wt% CNT	0.59	0.76
1.0 wt% CNT	0.43	0.70
1.5 wt% CNT	0.35	0.61

increase in the CNT loading. The increase in the storage modulus can be explained by the fact that the CNTs generate the percolated structure due to their high aspect ratio and high surface area. Fiber reinforced composites with high fiber volume fraction show the same result as the CNT nanocomposites. The epoxy composites filled with CNTs dispersed by using the solvent have much higher storage modulus than those filled with CNTs dispersed without the solvent. Terminal slopes of G' and G'' are listed in Table 1. As the CNT loading increases, the storage modulus exhibits a frequency independent solid like behavior at lower frequencies. Fig. 2 and Table 1 indicate that the nanocomposites do not show terminal behavior. The power-law dependence for G' is much smaller than the expected 2. In the case of poor dispersion of CNTs, more gradual decrease is observed in the slope of G' with respect to the CNT loading. It is attributed to the fact that the agglomerates in the poorly dispersed CNT nanocomposites act as large particles as if the filler loading were higher. The agglomerates trap polymer resin in the void between CNTs and the nanocomposites behave as if it had higher volume fraction of fillers. Differences in the terminal slopes are closely related to the internal structure of the nanocomposites which is affected by particle-particle interaction of the CNTs in the polymer matrix. Dynamic loss modulus, G'', of the nanocomposites is plotted in Fig. 3(a) and (b). It is known that the G' is more sensitive to morphology of particles than the G''. The loss modulus of the CNT/epoxy composite also shows different behavior with respect to the nanotube loading and the degree of dispersion. G' and G'' have the similar rheological behavior, i.e., Fig. 3 and Table 1 show non-terminal behavior of the loss modulus and the non-terminal behavior is more dominant in the case of poorly dispersed CNT/epoxy composites. Complex viscosity, $|\eta^*|$, of the CNT/epoxy composites is shown in Fig. 4. The epoxy composites filled with the poorly dispersed CNTs exhibit stronger non-Newtonian

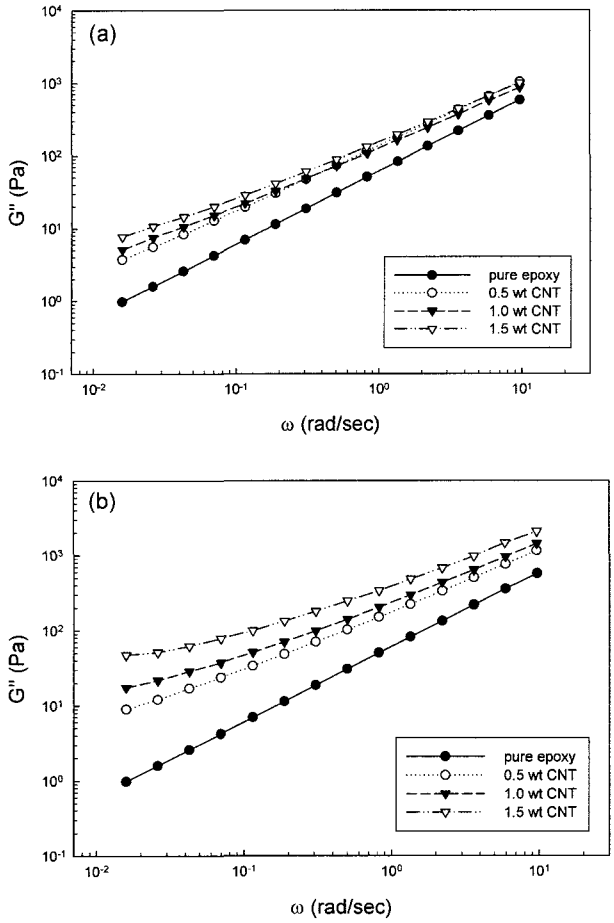

Fig. 3. Loss moduli of epoxy nanocomposites filled with (a) well dispersed CNTs and (b) poorly dispersed CNTs with respect to angular frequency.

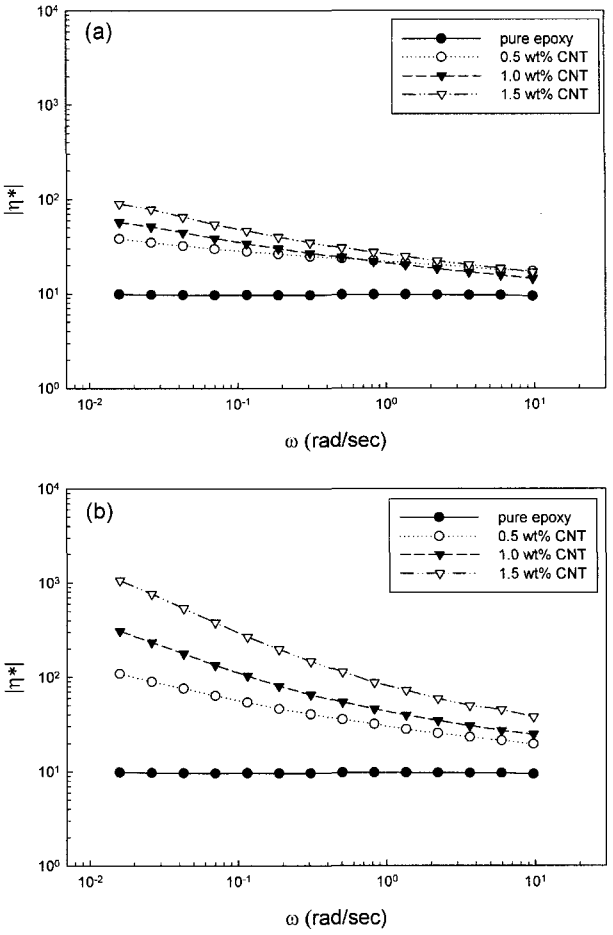

Fig. 4. Complex viscosities of epoxy nanocomposites filled with (a) well dispersed CNTs and (b) poorly dispersed CNTs.

behavior, close to the power law fluid, than those with the well dispersed CNTs. Viscosity of the former increases more rapidly with increase in the CNT loading. As the filler loading increases, interaction between the CNTs and the polymer resin becomes larger due to the high aspect ratio of the CNTs. The increase in the complex viscosity with respect to the CNT loading is primarily caused by the large increase in the storage modulus, G'. Steady state shear viscosity and the first normal stress coefficient of the nanocomposites with different dispersion states are plotted in Fig. 5 for 1 wt% CNT loading. The poorly dispersed CNT/epoxy composites have higher rheological material functions than the well dispersed ones both in the steady-state shear flow and in the oscillatory shear flow.

5.1.2. Morphology

TEM images of the CNTs dispersed in the epoxy resin are shown in Fig. 6 and Fig. 7. After conducting the tensile experiment of the CNT/epoxy composites, FESEM images of the fracture surface are shown in Fig. 8 and Fig. 9. The Figs. 6 and 8 show that the CNTs are relatively well dispersed in the epoxy resin. The CNTs are not broken but pulled out due to the weak interfacial bonding between the CNT and the polymer resin. The CNTs dispersed in the polymer without using the solvent exist in the form of agglomerates as shown in Fig. 7 and Fig. 9. The white regions in Fig. 9(a) represent the aggregated CNTs and the region is magnified as shown in Fig. 9(b) in order to verify the existence of CNTs. The agglomerates reduce reinforcing effects of the CNTs because they are acting as flaws in the resin. This is why the poorly dispersed CNT/epoxy composites have lower mechanical properties than the well dispersed ones.

5.2. Numerical results

5.2.1. Material functions in steady state shear flow

Calculated shear viscosity and first normal stress coefficient are shown in Figs. 10 and 11. Total 200000 FENE dumbbells and dimensionless time interval of 0.00001 were employed in the computation of bi-mode FENE dumbbell model. In order to verify the numerical data the results calculated when $c = 0$, which means that the proposed bi-mode FENE dumbbell is identical to the original

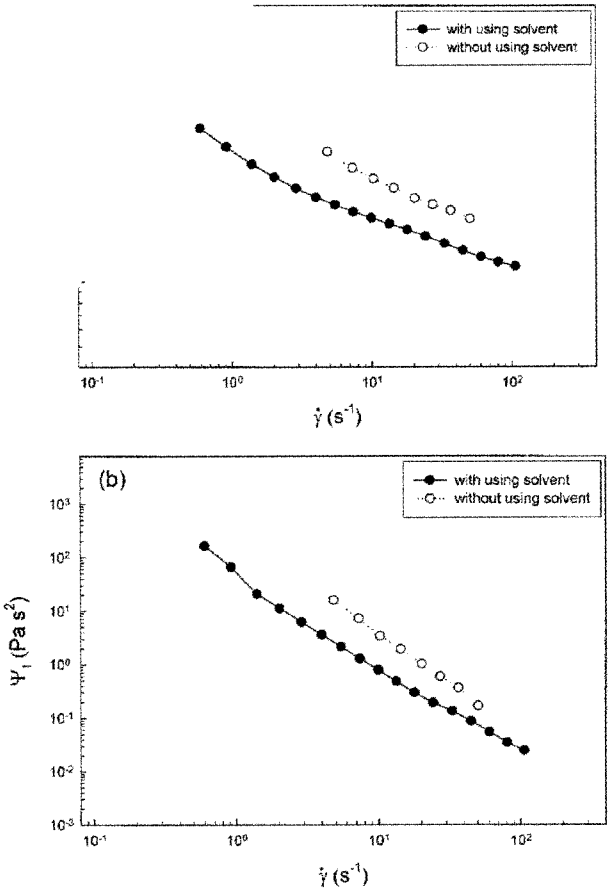

Fig. 5. (a) steady shear viscosity and (b) first normal stress coefficient of the CNTs/epoxy composites with respect to shear rate.

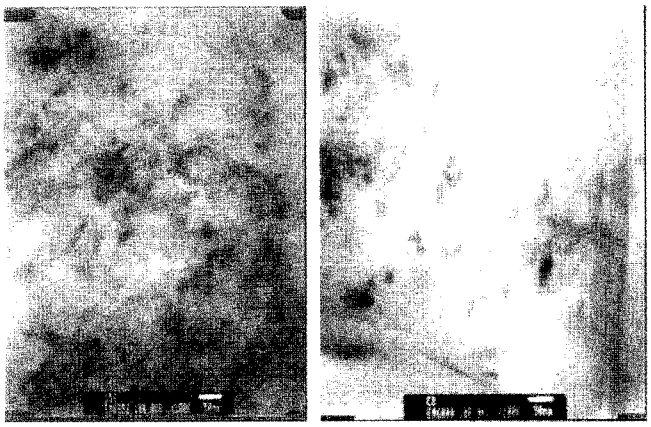

Fig. 6. TEM images of epoxy nanocomposites embedded with relatively well dispersed CNTs of 1.5 wt%.

FENE dumbbell model, were compared with those obtained by means of perturbation method. It is found that the aggregated FENE dumbbells with high c values, which represents the presence of aggregated fillers, have higher shear viscosities and first normal stress coefficients. Stress growth after inception of shear flow was analyzed by

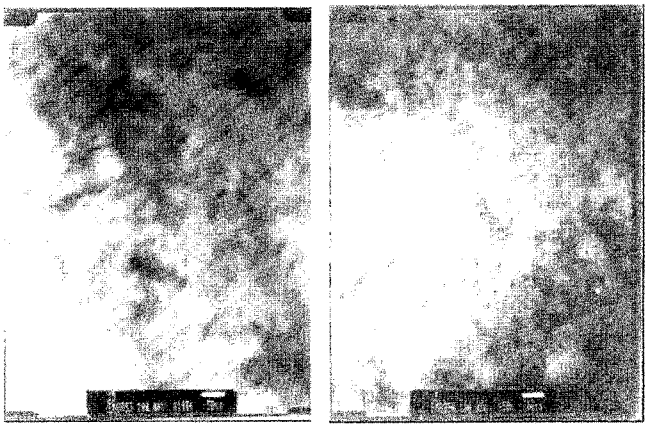

Fig. 7. TEM images of epoxy nanocomposites filled with poorly dispersed CNTs of 1.5 wt%.

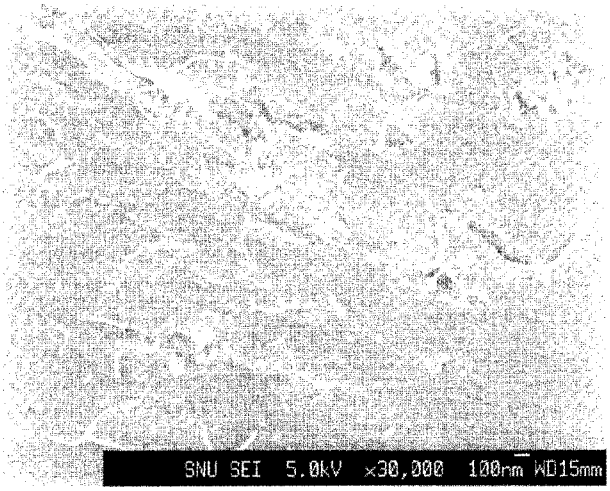

Fig. 8. FESEM images of the fracture surface for CNTs/ epoxy composites prepared by using a solvent.

assuming that the fluid was at rest before start-up and then the constant shear rate was applied. Growth of shear viscosity and first normal stress function is plotted with respect to dimensionless time in Figs. 12 and 13. The material functions in the steady state shear flow exhibit overshoot phenomena and have different steady state val with respect to the degree of dispersion. The overs occurs at the same time regardless of the CNT disp It is found that the shear viscosity is more sensiti CNT dispersion than the first normal stress co

5.2.2. Material functions in elongational

Elongational viscosities are plotted as a fur gation rate in Fig. 14. It is shown that the e cosity goes up with increase in the elong elongational viscosity of aggregated F higher than that of free FENE d results of bi-mode FENE dumbbell are in a good agreement with ana

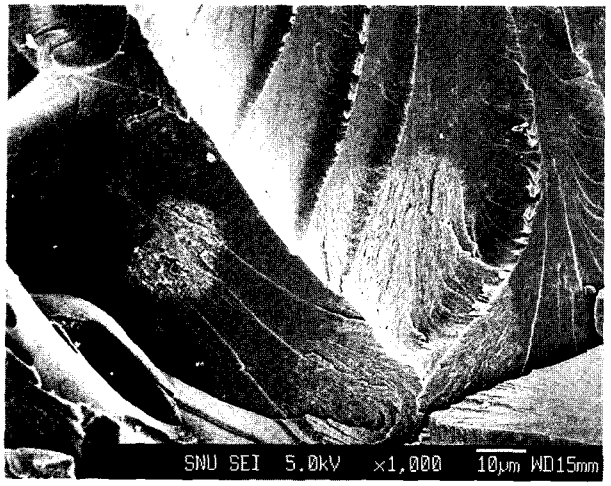

(a)

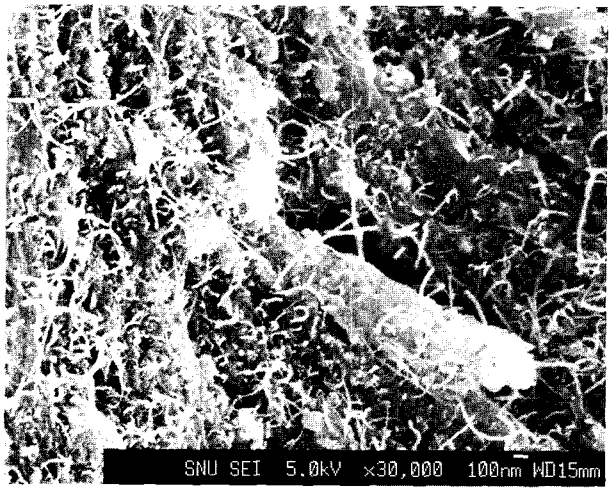

(b)

Fig. 9. FESEM images of CNTs/epoxy nanocomposites prepared without the solvent.

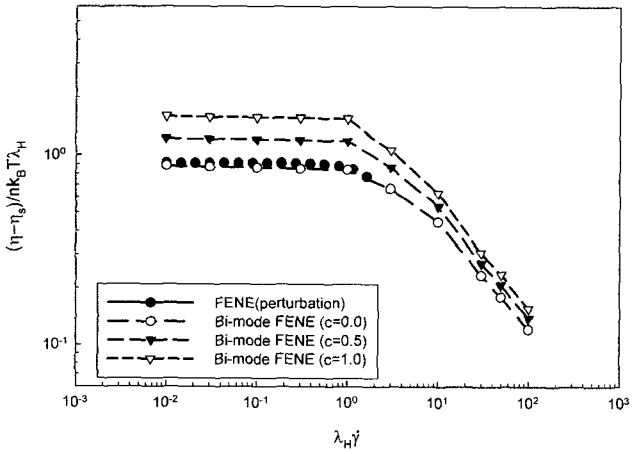

Fig. 10. Calculated shear viscosity as a function of shear rate for various dispersion states of the filler.

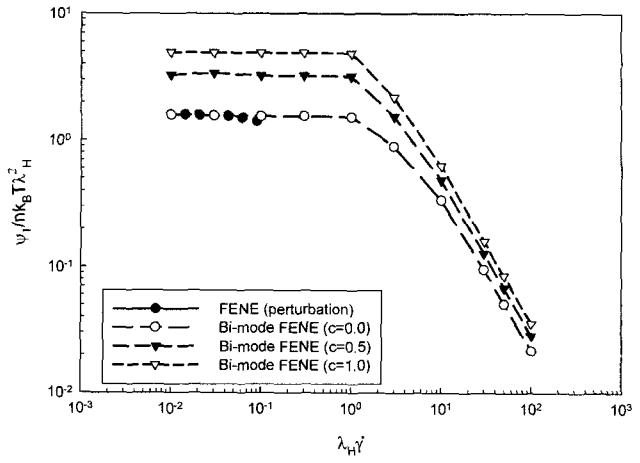

Fig. 11. Calculated first normal stress coefficient as a function of shear rate for various dispersion states of the filler.

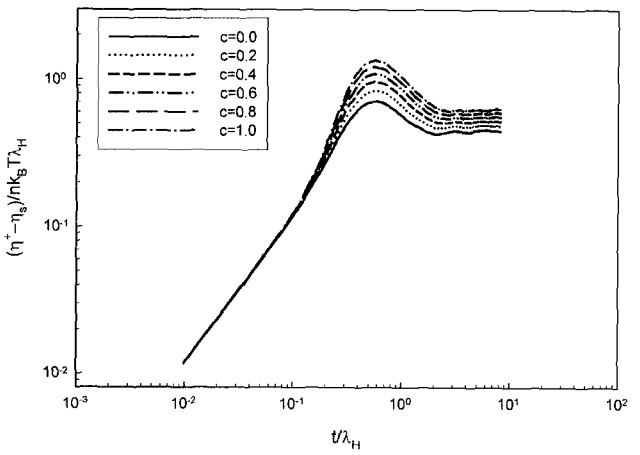

Fig. 12. Growth of shear viscosity after inception of shear flow when dimensionless shear rate is $\lambda_H\dot{\gamma}=10$.

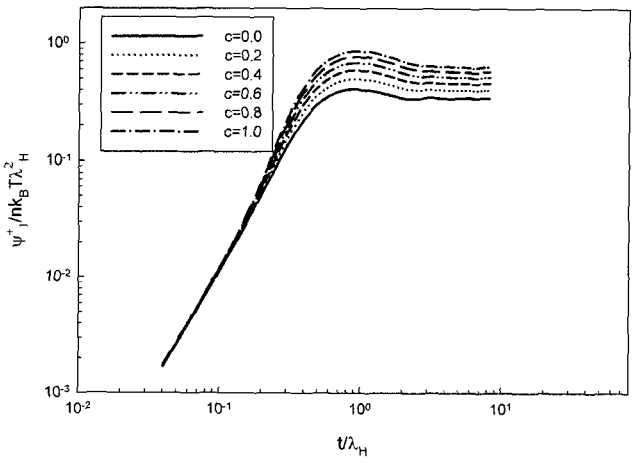

Fig. 13. Growth of first normal stress coefficient after inception of shear flow when dimensionless shear rate is $\lambda_H\dot{\gamma}=10$.

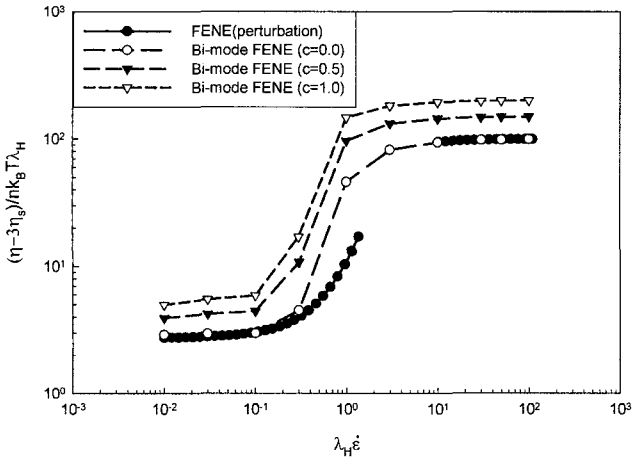

Fig. 14. Elongational viscosity calculated as a function of elongation rate by using bi-mode FENE dumbbells.

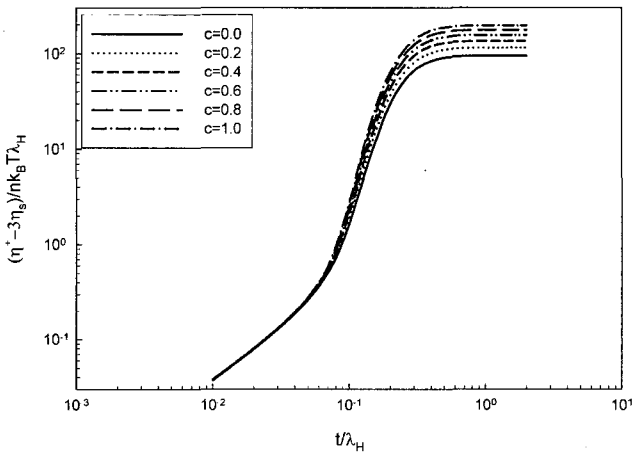

Fig. 15. Time evolution of elongational viscosity after inception of elongational flow when dimensionless elongation rate is $\lambda_H\dot{\varepsilon} = 10$.

iting range of elongation rate. Growth of the viscosity after inception of elongational flow for the various dispersion states is shown in Fig. 15. As the number of aggregated FENE dumbbells increases, higher steady elongational viscosity is obtained. As seen in Fig. 16, the elonational viscosities increase until they reach steady state. Higher strain hardening behavior is observed as the elongation rate increases. Figs. 17 and 18 show radial distributions of aggregated and free FENE dumbbell lengths in the start-up of elongational flow. After the flow is started from the equilibrium state, the radial distribution of the dumbbell length evolves toward steady state with respect to time toward steady state. Since the aggregated FENE dumbbells have a higher friction coefficient, they are subject to larger friction force against the applied flow field. As a results, they have higher radial dumbbell length and narrower distribution of length than free dumbbells. It is also verified

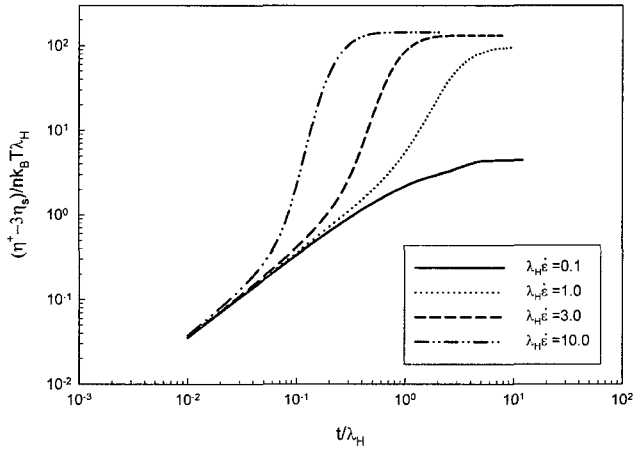

Fig. 16. Time evolution of elongational viscosity after inception of elongational flow when $c = 0.5$.

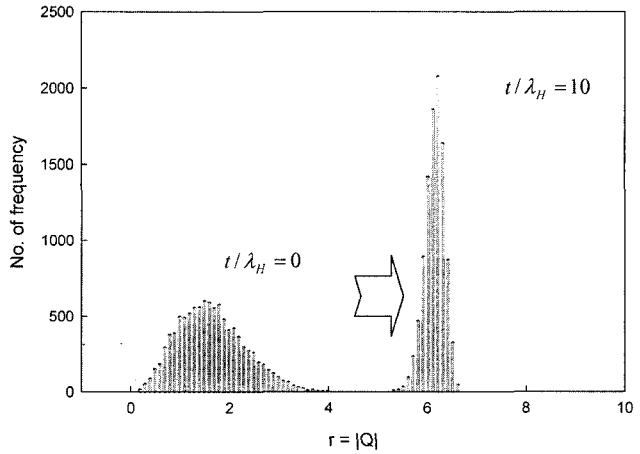

Fig. 17. Change in distribution of aggregated FENE dumbbell length after start-up of elongational flow when dimensionless elongation rate is 1.0.

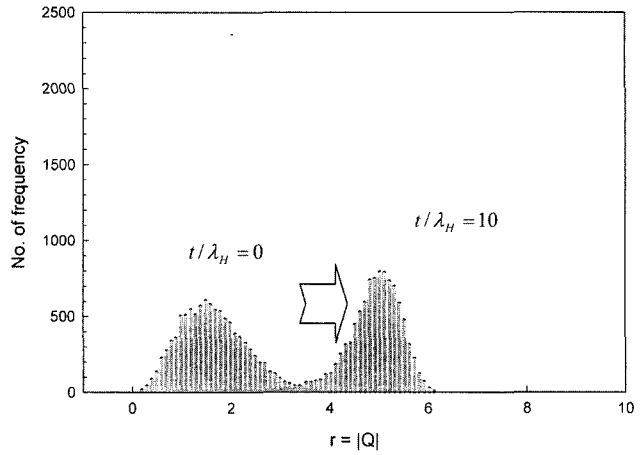

Fig. 18. Change in distribution of free FENE dumbbell length after start-up of elongational flow when the number of dumbbell is 10,000 and dimensionless elongation rate is 1.0.

that the radial dumbbell length in the FENE dumbbell model can not exceed $\sqrt{b}$ that is the upper limit (in this study, $b = 50$).

5.2.3. Material functions in small amplitude oscillatory flow

The predicted storage modulus increases with increase in the degree of dispersion as shown in Fig. 19. Generally, it is known that the polymer solution filled with aggregated particles has higher storage modulus than that with well dispersed particles and the storage modulus has a solid like behavior at low frequency [19]. The bi-mode FENE dumbbell model can account for the increment of storage modulus in polymer systems containing the aggregated fillers. However, the model fails to depict solid like behavior of storage modulus, which is caused by original limitation of the FENE dumbbell. Fig. 20 shows the effect of dispersion state on the loss modulus. The loss modulus of free FENE dumbbells is higher than that of aggregated FENE dumbbells in the range of high frequency, i.e., high deformation rate.

5.3. Comparison between numerical and experimental results

The results predicted and measured in the case of steady state shear flow are compared as shown in Fig. 21. The predicted shear viscosity has a good agreement with experimental data as shown in Fig. 21(a). That is, the aggregated FENE dumbbells and CNT nanocomposites exhibit higher shear viscosities than free FENE dumbbells and well dispersed CNT nanocomposites. The calculated data were fitted based on the assumption that relaxation time λ_H of the aggregated FENE dumbbell is twice as long as that of the free FENE dumbbell since $\zeta_f/\zeta_a = 0.5$. It is indicated that the parameter c successfully represents degree of CNT dispersion for nanocomposites in the steady state shear flow quantitatively. The first normal stress coefficients plotted in Fig. 21(b) show that there is a little discrepancy between

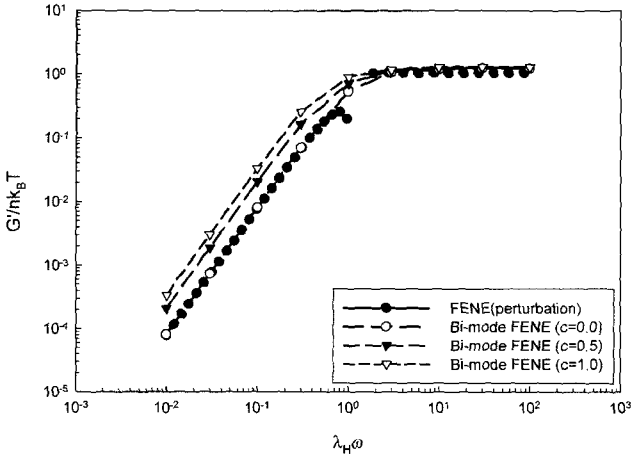

Fig. 19. Storage modulus calculated as a function of frequency by using bi-mode FENE dumbbells.

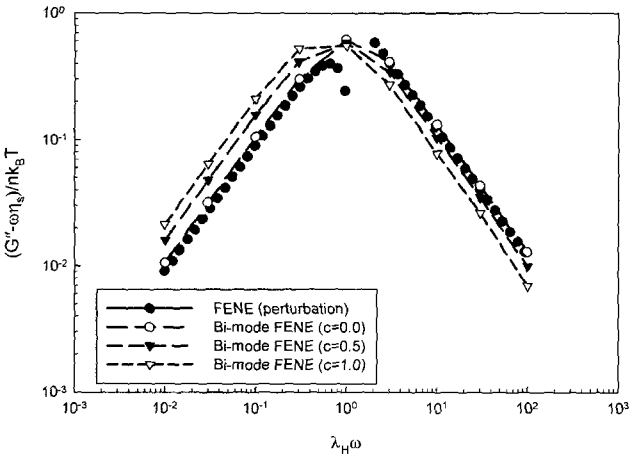

Fig. 20. Loss modulus calculated as a function of frequency by using bi-mode FENE dumbbells.

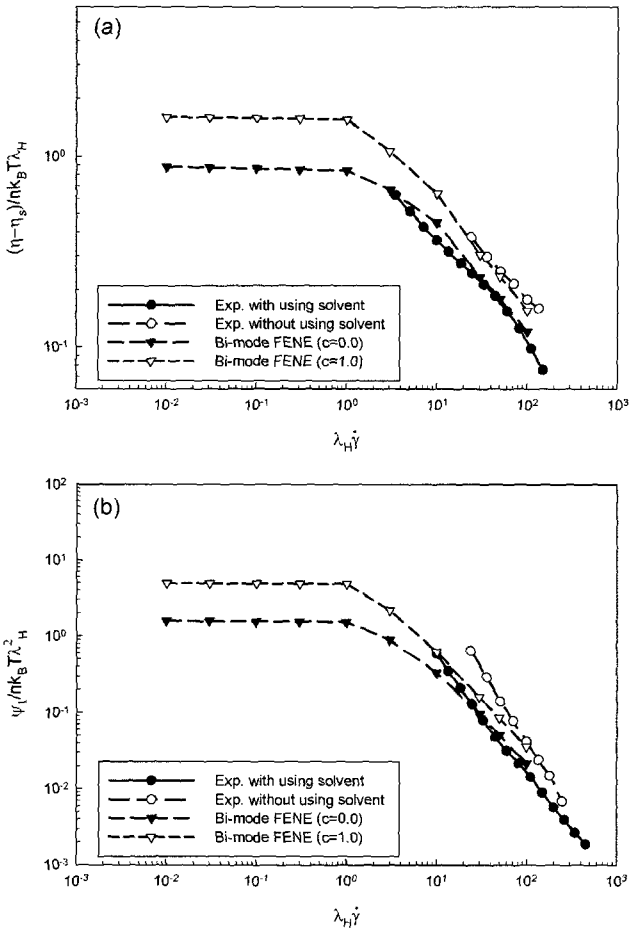

Fig. 21. Comparison between predicted and measured (a) steady shear viscosities and (b) first normal stress coefficients. The dumbbell data are fitted based on $\lambda_H = 2.48$ s and $nk_BT = 8.3$ Pa·s.

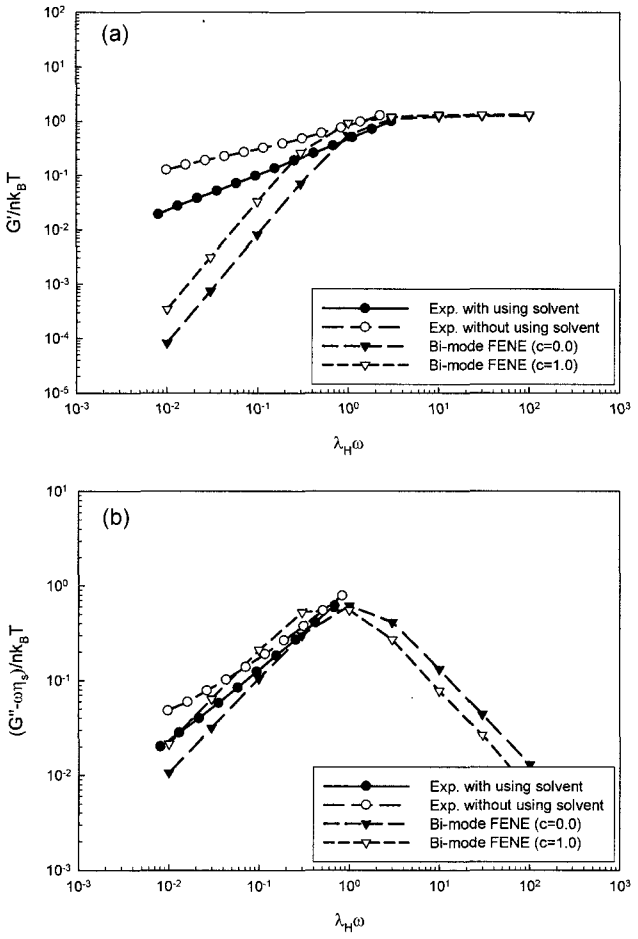

Fig. 22. Comparison between predicted and measured (a) storage moduli and (b) loss moduli. The dumbbell data are fitted based on $\lambda_H = 0.31$ s and $nk_BT = 210$ Pa·s.

the predicted and experimental slopes. However, the aggregated FENE dumbbells or aggregated CNTs still have higher first normal stress coefficients than the free ones. As a result, the bi-mode FENE dumbbell model can successfully describe the influence of the CNT dispersion on the material functions in the steady state shear flow quantitatively as well as qualitatively. On the other hand, it is known that original FENE dumbbells depict the dependence of shear viscosity on the shear rate well but do not provide material functions quantitatively in the oscillatory shear flow.

Fig. 22(a) and (b) present storage and loss moduli. The calculated results are different from the experimental data. Especially, the storage modulus obtained by using the bi-mode FENE dumbbell is overestimated in the range of low frequency. However, the bi-mode FENE dumbbells are able to capture convergence of the modulus values between aggregated and well dispersed CNT nanocomposites with respect to frequency and explain dependence of storage and loss moduli on the CNT dispersion.

6. Conclusions

In order to examine the influence of CNT dispersion on the rheological behavior of the CNT filled composites, two different specimens with the well dispersed and the poorly dispersed CNTs were prepared depending on whether solvent was used during the CNT dispersion process. The rheological properties of the nanocomposites were experimentally examined with respect to the weight fraction of the CNTs. Dispersion state of the CNT in the epoxy nanocomposites was characterized morphologically by the field emission scanning electronic microscope and the transmission electron microscope. It was found by the experiment that the nanocomposites containing the poorly dispersed CNTs exhibit higher storage modulus, loss modulus, and complex viscosity than those with the well dispersed CNTs. To describe the effect of the CNT dispersion state on the rheological properties numerically, Brownian dynamics simulation based on stochastic differential equation was performed. A new bi-mode FENE dumbbell model was proposed. Material functions in the elongational, steady shear, and oscillatory shear flows were computed numerically and compared with measured ones. It was shown that the model depict rheological behavior of the CNT nanocomposites successfully and the new parameter c can represent the degree of dispersion of filled particles quantitatively.

Acknowledgements

This study was partially supported by the Korea Science and Engineering Foundation through the Applied Rheology Center (ARC) and by the Ministry of Science and Technology through the National Research Laboratory. The authors are grateful for the support.

References

Allaoui, A., S. Bai, H.M. Cheng and J.B. Bai, 2002, Mechanical and Electrical Properties of a MWNT/Epoxy Composites, *Compos. Sci. Tech.* **62**, 1993.

Armstrong, R.C. and S. Ishikawa, 1980, A Rheological Equation of State for Dilute Solutions of Nearly-Hookean Dumbbells, *J. Rheol.* **24**, 143.

Bird, R.B. and J.R. Deaguiar, 1983, An Encapsulated Dumbbell Model for Concentrated Polymer Solutions and Melts. I. Theoretical Development and Constitutive Equation, *J. Non-Newtonian Fluid Mech.* **13**, 149.

Bird, R.B. and J.M. Wiest, 1985, Anisotropic Effects in Dumbbell Kinetic Theory, *J. Rheol.* **29**, 519.

Bird, R.B., C.F. Curtiss, R.C. Armstrong and O. Hassager, 1987, *Dynamics of Polymeric Liquids: Volume 2, Kinetic Theory*, John Willy & Sons, New York.

Christiansen, R.L. and R.B. Bird, 1977/1978, Dilute Solution Rheology: Experimental Results and Finitely Extensible Non-

linear Elastic Dumbbell Theory, *J. Non-Newtonian Fluid Mech.* **3**, 161.

Fan, X.J., 1985, Viscosity, First Normal-Stress Coefficient, and Molecular Stretching in Dilute Polymer Solutions, *J. Non-Newtonian Fluid Mech.* **17**, 125.

Hernández Cifre, J.G., Th.M.A.O.M. Barenbrug, J.D. Schieber and B.H.A.A. van den Brule, 2003, Brownian Dynamics Simulation of Reversible Polymer Networks under Shear Using a Non-Interacting Dumbbell Model, *J. Non-Newtonian Fluid Mech.* **113**, 73.

Kinloch, I.A., S.A. Roberts and A.H. Windle, 2002, A Rheological Study of Concentrated Aqueous Nanotube Dispersions, *Polymer*, **43**, 7483.

Larson, R.G., 1988, *Constitutive Equations for Polymer Melts and Solutions*, Butterworths, AT&T, Boston.

Öttinger, H.C., 1994, Variance Reduced Brownian Dynamics Simulations, *Macromolecules* **27**, 3415.

Öttinger, H.C., 1996, *Stochastic Processes in Polymeric Fluids*, Springer, Berlin.

Öttinger, H.C., B.H.A.A. van den Brule and M.A. Hulsen, 1997, Brownian Configuration Fields and Variance Reduced CONNFFESSIT, *J. Non-Newtonian Fluid Mech.* **70**, 255.

Pötschke, P., T.D. Fornes and D.R. Paul, 2002, Pheological Behavior of Multiwalled Carbon Nanotube/Polycarbonate Composites, *Polymer* **43**, 3247.

Schieber, J.D., 1993, Internal Viscosity Dumbbell Model with a Gaussian Approximation, *J. Rheol.* **37**, 1003.

Shaffer, M.S.P., X. Fan and A.H. Windle, 1998, Dispersion and Packing of Carbon Nanotubes, *Carbon* **36**, 1603.

Shenoy, A.V., 1999, *Rheology of Filled Polymer Systems*, Kluwer Academic Publishers, Dordrecht.

Vaccaro, A. and G. Marrucci, 2000, A Model for the Nonlinear Rheology of Associating Polymers, *J. Non-Newtonian Fluid Mech.* **92**, 261.

Warner Jr., H.R., 1972, Kinetic Theory and Rheology of Dilute Suspensions of Finitely Extensible Dumbbells, *Ind. Eng. Chem. Fundam.* **11**, 379.